Analysis of $\eta\pi^0$ system with the decay $\eta \to \pi^+\pi^-\pi^0$ Part 1

V.L.Korotkikh, L.V. Malinina

14 July 2005

E852 collaboration

Scobeltsyn Institute of Nuclear Physics
Moscow State University, 119992 Moscow, Russia

Abstract

The exclusive reaction $\pi^- p \to \eta\pi^0 n$, $\eta \to \pi^+\pi^-\pi^0$, $\pi^0 \to 2\gamma$ at 18 GeV/c has been studied in E852 experiment. A partial wave analysis has been performed on a sample of 23492 $\eta\pi^0 n$ events. A mass dependent fit with the average ambiguous solutions and a mass dependent partial wave analysis give the coincident resonant parameters of the P_+ wave. We have an evidence of neutral exotic $J^{PC} = 1^{-+}$ meson state $\pi_1^0(1400)$.

Introduction

In our previous works [1], [2] we reported evidence for an exotic $J^{PC} = 1^{-+}$ resonance state $\pi_1(1400)$ in the reaction $\pi^- p \to \eta\pi^- p$, $\eta \to 2\gamma$. The Crystal Barrel experiment [3] confirmed this result for $\eta\pi^-$ system in the reaction with antiprotons stopped in liquid deuterium, $\bar{p}n \to \pi^-\pi^0\eta$. Later this group analysed the data on $\bar{p}p$ annihilation at rest into $\pi^0\pi^0\eta$ [4] and presented evidence for the exotic 1^{-+} resonance in $\eta\pi^0$ system with $M = (1360 \pm 25)$ MeV/c^2 and $\Gamma = (220 \pm 90)$ MeV/c^2.

The state $\eta\pi^0$ has been studied by the GAMS experiment [5] in the reaction $\pi^- p \to \eta\pi^0 n$, $\eta \to 2\gamma$, $\pi^0 \to 2\gamma$ at 32, 38 and 100 GeV/c. They showed that the P_+ wave mass dependence has a wide bump at $M = 1300$

MeV/c^2. Its form depends strongly on the ambiguous solutions. Large statistic at 38 GeV/c allows to use the original method of the physical solution selection [6] and to find an exotic meson $\pi_1(1400)$.

Analysis of the reaction $\pi^- p \to \eta\pi^0 p$, $\eta \to 2\gamma$ in E852 experiment was performed in work [7]. A bump in P_+ wave of $\eta\pi^0$ system is observed at $M(\eta\pi^0) = 1272 MeV$ with large width $\Gamma = 660 MeV$. The strong dependence of resonant parameters of P_+ wave on different t' intervals doesn't allow to claim the evidence of exotic $\pi_1(1400)$ meson.

We have studied the reaction $\pi^- p \to \eta\pi^0 n$, $\eta \to \pi^+\pi^-\pi^0$, $\pi^0 \to 2\gamma$ at 18 GeV/c. The important and obvious characteristic of the $\eta\pi^0$ system unlike $\eta\pi^-$ system is that C-parity is a good quantum number. Thus it is possible to study a neutral exotic (non $q\bar{q}$) state with quantum numbers $J^{PC} = 1^{-+}$.

The other distinguishing feature of the charge exchange reaction $\pi^- p \to \eta\pi^0 n$ is that the production mechanism cannot involve the exchange of an isospin $I = 0$ system and thus pomeron exchange is ruled out. Finally, it is important to note that, from the experimental point of view, in the reaction $\pi^- p \to \pi^+\pi^- 4\gamma n$ we can define the interaction point by the charged tracks and convince ourself that the event is in the target region. This is not possible in the all neutral final state when the η decays to 2 photons.

The data for this analysis was obtained in the E852 experiment at the Alternating Gradient Synchrotron (BNL USA) during 1995. Using an 18 GeV/c π^- beam interacting with liquid hydrogen targe, a total of 750 million triggers were acquired of which 108 million were of a type designed to enrich the exclusive final state events $\pi^- p \to \pi^+\pi^- 4\gamma n$. A total 6 million events of this type were fully reconstructed. The data were kinematically fitted to select events consistent with an $\pi^-\pi^+\pi^0\pi^0 n$ hypothesis. 3973000 events were fully reconstructed. After mass cut $m(\pi^-\pi^+\pi^0) < 0.65 GeV$ we have 85228 events and after ellips cut (where the drift chamber efficiency was low for run 1995 year) 74549 events of $\pi^-\pi^+\pi^0\pi^0 n$.

Then the data were kinematically fitted to select 31679 events consistent with an $\eta\pi^0 n$ hypothesis. Requiring a minimum acceptable confidence level of 1% for this hypothesis, a total of 23492 $\eta\pi^0 n$ events remained for the partial wave analysis (PWA).

1 Production vertex and the charge tracks in TPX1 and TPX2

The charge particles π^+ and π^- allow us to set that a production vertex is in the region of target (see Fig. 1 and Fig. 2).

We have performed the cuts of the charge tracks in TPX1 and TPX2 detectors because the drift chamber efficiency was low for run 1995 year (see, for example, Fig. 3 for TPX1)

2 Cut of mass

The cut mass $m(\pi^0\pi^+\pi^-) < 0.65GeV$ is presented in Fig.5. Two dimension plot of the data events with that cut and kinematically fitted with an $(\eta\pi^0)$ hypothesis is in Fig. 6.

The mass distributions of two pions before and after cut mass $m(\pi^0\pi^+\pi^-) < 0.65GeV$ are in Fig. 7.

Three pion, four pion mass distributions, t' - and and $cos(\theta_{GJ})$ distributions before and after cut mass $m(\pi^0\pi^+\pi^-) < 0.65GeV$ are in Fig. 8.

3 Background of $\eta\pi^0$ distribution

A signal of η meson is shown in Fig. 9. The fit by a sum of Gaussian and polinomial background gives the parameters of mass $539.2 \pm 0.3MeV$ and width of $23.7 \pm 0.22MeV$. The mass value corresonds to the published values. The value of $\Gamma \simeq 24MeV$ is our experimental resolution of mass $\pi^0\pi^+\pi^-$ system. Ratio of η signal to the bacground is 6 to 1 for the whole mass $m(\eta\pi^0)$ considered.

Selection of the side bands near η signal is in fig. 10.

We calculated background (see Fig. 11), using the side bands . A ratio Bcgr/Data is in Fig. 12 for different mass bins of $\eta\pi^0$ system, which were used in PWA.

The ratio is equal to 0.17 in average in mass region 0.8 - 1.7 GeV.

4 Distributions for $\eta\pi^0$ system

The main distributions are in Fig. 13.

The dependence of $\eta\pi^0$ system mass shows two well-defined peaks at 1.0 and 1.3 MeV/c^2. Mass distributions on Fig. 13c show that the cuts

on $cl > 0.01$ and $cl > 0.05$ give the same form of mass distribution. So we use $cl > 0.01$ to save more large statistics (23492 events) in PWA. The comparison of mass distribution in the whole t' - region and at $t' > 0.1(GeV/c)^2$ is in Fig. 13d. A few change of mass distribution is seen.

5 Acceptance of $\eta\pi^0$ system distributions

Acceptance of mass($\eta\pi^0$) and t' - distributions are shown in fig. 14. Note, that these acceptance distribution are very flat.

Acceptance of $cos_{GJ}(\eta\pi^0)$ and $\phi_{TY}(\eta\pi^0)$- distributions are shown in fig. 15.

6 t' - distributions

We fit the t'-dependence of the acceptance corrected data for all masses (see Fig. 16), using the expression

$$N(t') = n_1|t'|e^{-b_1|t'|} + n_2 e^{-b_2|t'|}.$$

A first term in sum is a our natural parity exchange (NPE) contribution with spin projectiom M=1 and the second term is an unnatural parity exchange (UNPE) contribution with dominant M=0 waves.

We find the next parameters

$$b_1 = (7.41 \pm 0.08)(\mathrm{GeV/c})^2, \qquad b_2 = (2.68 \pm 0.07)(\mathrm{GeV/c})^2.$$

$$n_2/n_1 = 0.71 \pm 0.03$$

.

The difference betwen $b_1 = 7.41(\mathrm{GeV/c})^2$ and $b_2 = 2.68(\mathrm{GeV/c})^2$ and the ratio $n_2/n_1 = 0.71$ at $18GeV/c$ corresponds to Regge trajectories for ρ and b_1 reggions accordingly to NPE and UNPE.

7 Angular distributions in the η and side bands mass regions

We show the angular distributions $\cos(\theta_{GJ})$ and ϕ_{TY} in the region of η signal and in the side bands in Fig.17 (two dimension plots) and Fig.18 (projection on $\cos(\theta_{GJ})$ and ϕ_{TY}). The distributions are considerable flat for the side bands, thought statistics is small.

8 Partial Wave Analysis

The PWA was performed on the sample of 23492 $\eta\pi^0 n$ events (note that for $\eta\pi^- p$ events [2] there were 47200 events) for $0.78 < M(\eta\pi^0) < 1.72$ GeV/c^2 and $0. < |t'| < 1.0$ (GeV/c)^2 in $\Delta M = 40$ MeV/c^2 mass bins. The PWA has been done using 7 amplitudes: S_0, P_0, P_-, D_0, D_- (unnatural parity exchange, UNPE) and P_+, D_+ (natural parity exchange).

The D_+ and P_+ waves are the main contributions to the total intensity. The ratio of P_+ and D_+ wave intensities is greater (about 30%) than for the $\eta\pi^-$ system (about 5%) [2]. The same ratio is observed for the $\eta\pi^0$ system in the GAMS analysis. The contribution of the seperate UNPE waves is smaller ($< 20\%$) then for the P_+ wave , but the spread of the UNPE ambiguous solutions is larger than for the $\eta\pi^-$ system . For this reason, the shape of the P_+ intensity distribution depends strongly on solution selection.

The goodness-of-fit for the PWA is good. The comparison of the data moments $H(LM)$, $(L \leq 2, M \leq 2)$ and their prediction from the PWA are shown in Fig. 19. We also compare the data and MC predicted $cos(\theta_{GJ})$ and φ_{TY} distributions in Fig. 20.

The results of PWA with all ambiguous solutons are presented in Fig. 21 and Fig. 22.

We fit a mass dependence of the intensities of the D_+ and P_+ waves and their relative phase in the region $1.10 < M(\eta\pi^0) < 1.74$ GeV/c^2. See Fig. 23. The values for the intensities and phases are taken from the PWA as the average values of the ambiguous solutions. The errors are calculated from the average error matrix. The mass dependent fit includes a Breit-Wigner (BW) amplitude for the D_+ wave with a second order polynomial background, a BW amplitude for the P_+ wave (resonant hypothesis) and a mass-independent production phase. For the nonresonant hypothesis we used a BW intensity distribution for the P_+ wave without resonant phase.

The result of the fit with the resonant hypothesis ($\chi^2/dof = 1.22$) is in shown in Fig. 23. There is no need to introduce a mass dependence for the production phase in the resonant hypothesis. The detailed results of Breit-Wigner mass dependent fit and the systematic study are presented in our note [8].

The parameters of the fitted BW amplitudes for the 2^{++} state (a_2^0 meson) are

$$M(a_2^0) = (1320 \pm 3^{+10}_{-7}) \text{ MeV/c}^2,$$

$$\Gamma(a_2^0) = (96 \pm 3^{+40}_{-15})\ \mathrm{MeV/c^2},$$

The parameters of the exotic 1^{-+} state (π_1^0 meson) are

$$M(\pi_1^0) = (1270 \pm 14^{+80}_{-70})\ \mathrm{MeV/c^2},$$
$$\Gamma(\pi_1^0) = (334 \pm 42^{+116}_{-184})\ \mathrm{MeV/c^2}.$$

The systematic errors for the mass and width are taken from the range of the random fit of arbitrary combinations of ambiguous solutions (see [8]).

References

[1] D.R. Thompson *et al.*, Phys. Rev. Lett. **79**, 1630 (1997).

[2] S.U. Chung *et al.*, Phys. Rev. D **60**, 092001 (1999).

[3] A. Abele *et al.*, Phys. Lett. B **423**, 175 (1998).

[4] A. Abele *et al.*, Phys. Lett. B **446**, 349 (1999).

[5] A.Lednev, Proceedings of 7-th Int. Conf. on Hadron Spectroscopy, Upton, **NY**, 253 (1977)

[6] S.A. Sadovsky, Nucl. Phys. A **655**, 131c (1999).

[7] A.R. Dzierba *et al.*, Phys. Rev. D **67**, 094015 (2003).

[8] V.L. Korotkikh, L.V. Malinina, Mass dependent fit of PWA results for $\eta\pi^0$ system. Part 2. (2005)

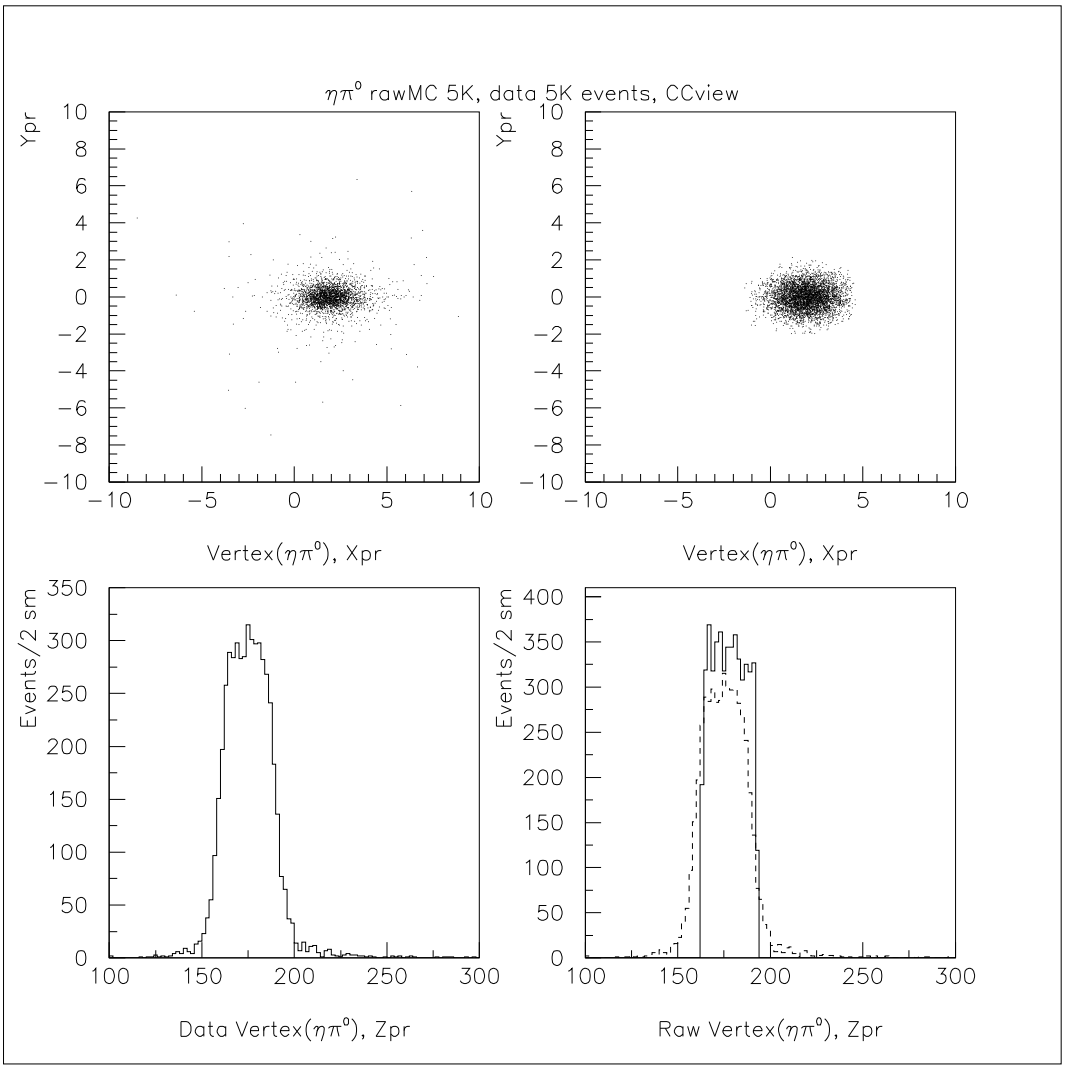

Figure 1: Production vertex. Left coulomb is data events, rigth coulomb is MC events. Low raw is z coordinate of producton vertex. Dotted line on the right is data from the left

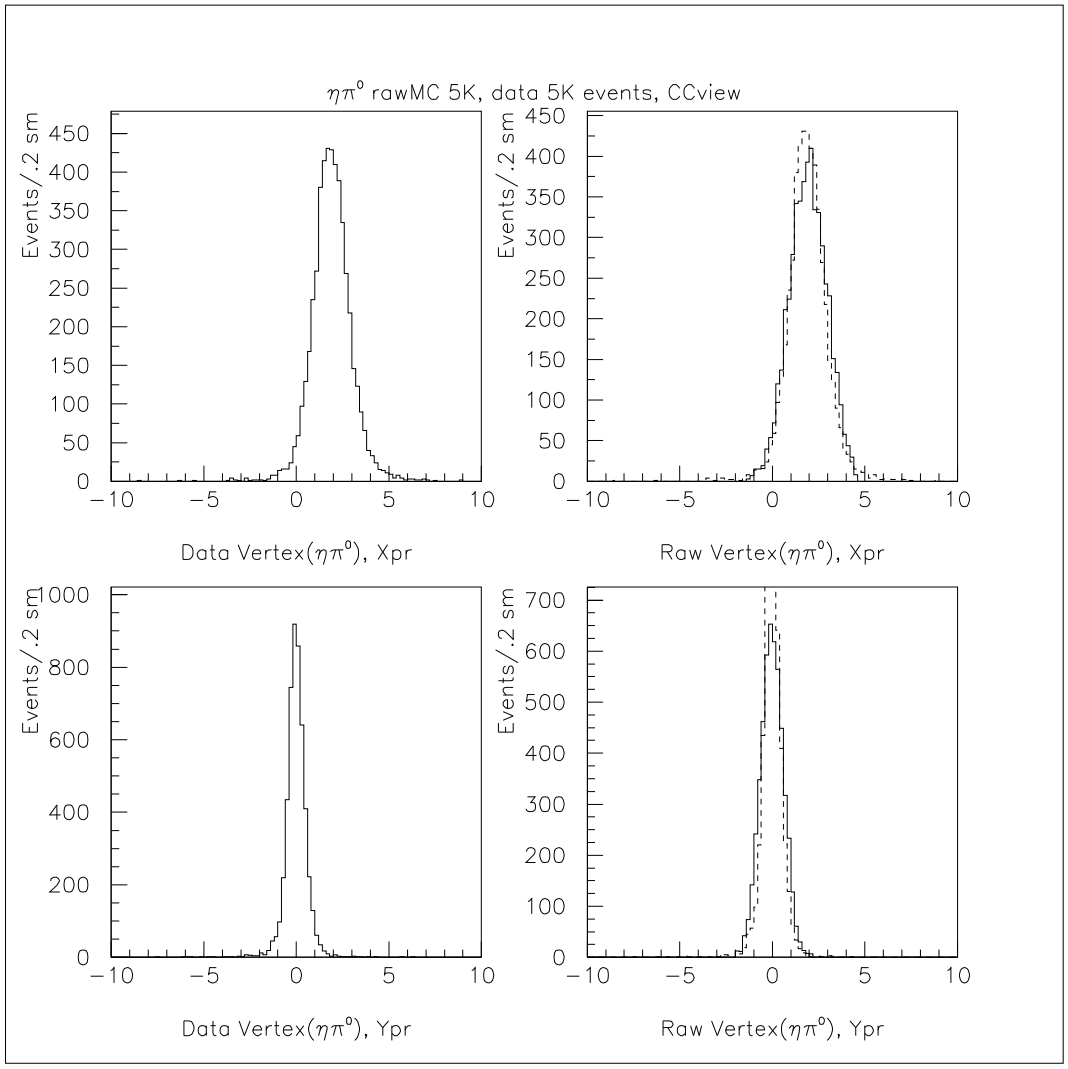

Figure 2: Production vertex. x and y coordinates of producton vertex. Dotted line on the right is data from the left

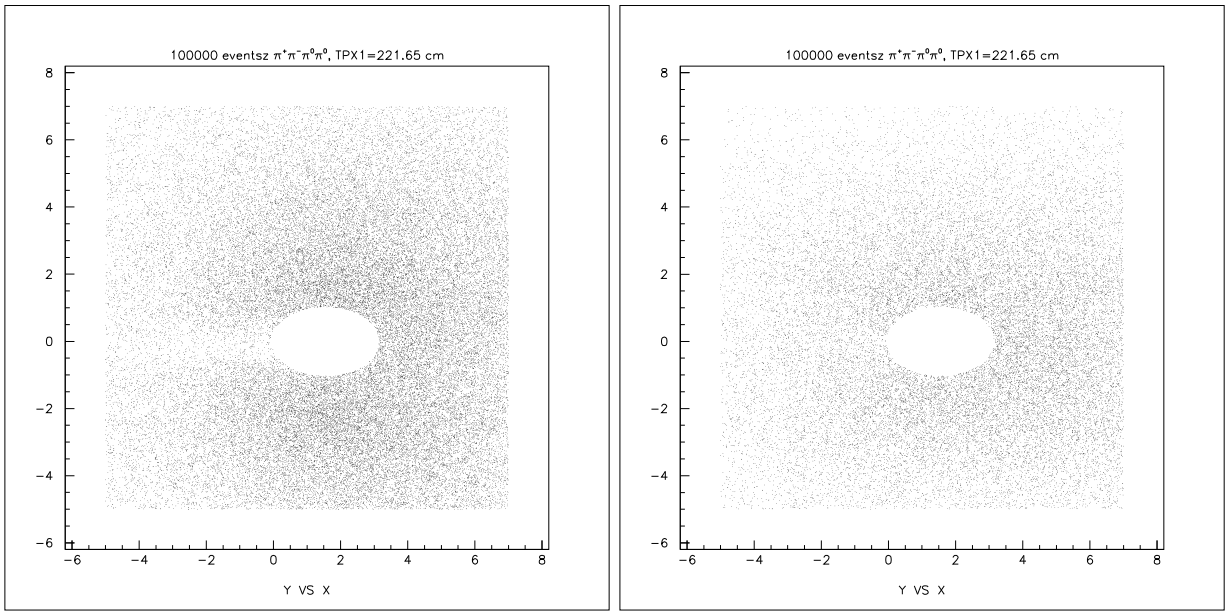

Figure 3: Charge tracks for data events in TPX1 detector with elliptical cut in the beam region

Figure 4: Charge tracks for MC events in TPX1 detector with elliptical cut in the beam region

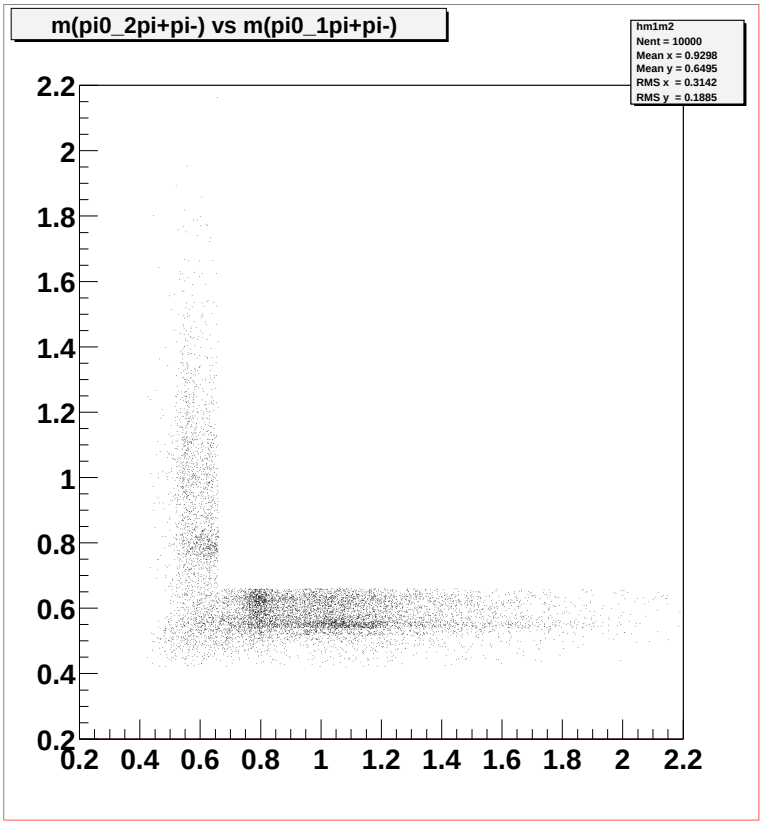

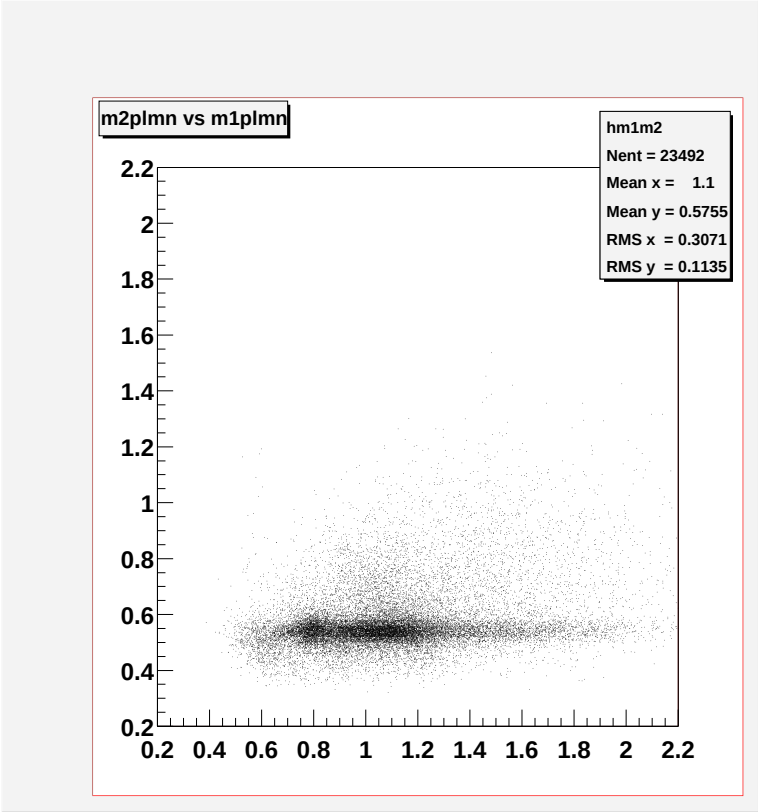

Figure 5: Sample of 10000 events, two demension plot of mass $(\pi^0\pi^+\pi^-)$ distribution at mass cut $m(\pi^0\pi^+\pi^-) < 0.65GeV$

Figure 6: Two demension plot of mass($\pi^0\pi^+\pi^-$) after mass cut $m(\pi^0\pi^+\pi^-) < 0.65GeV$ and SQUAW $(\eta\pi^0)$

.

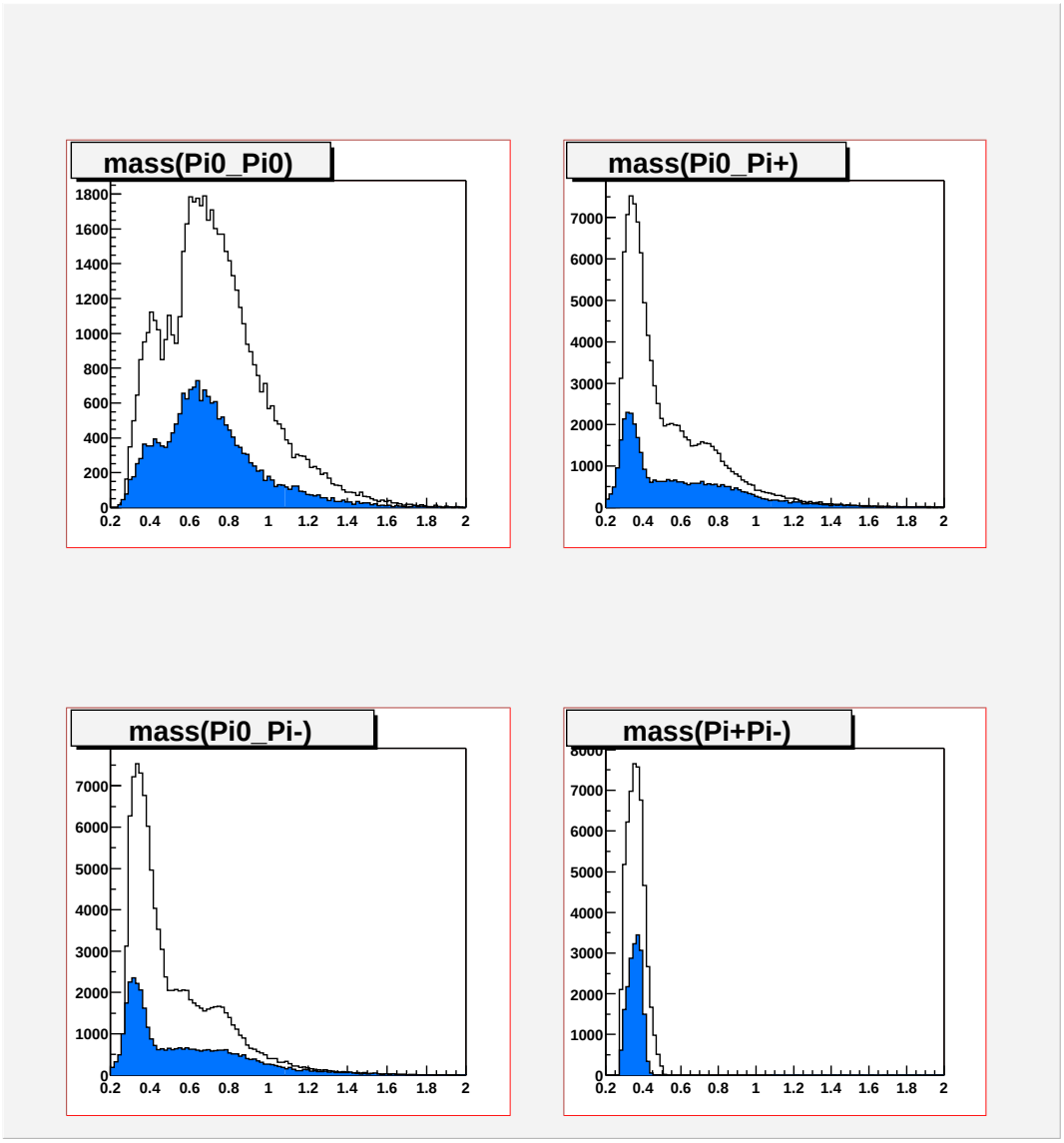

Figure 7: Two pions mass distributions. Hatched histogrames are after mass cut

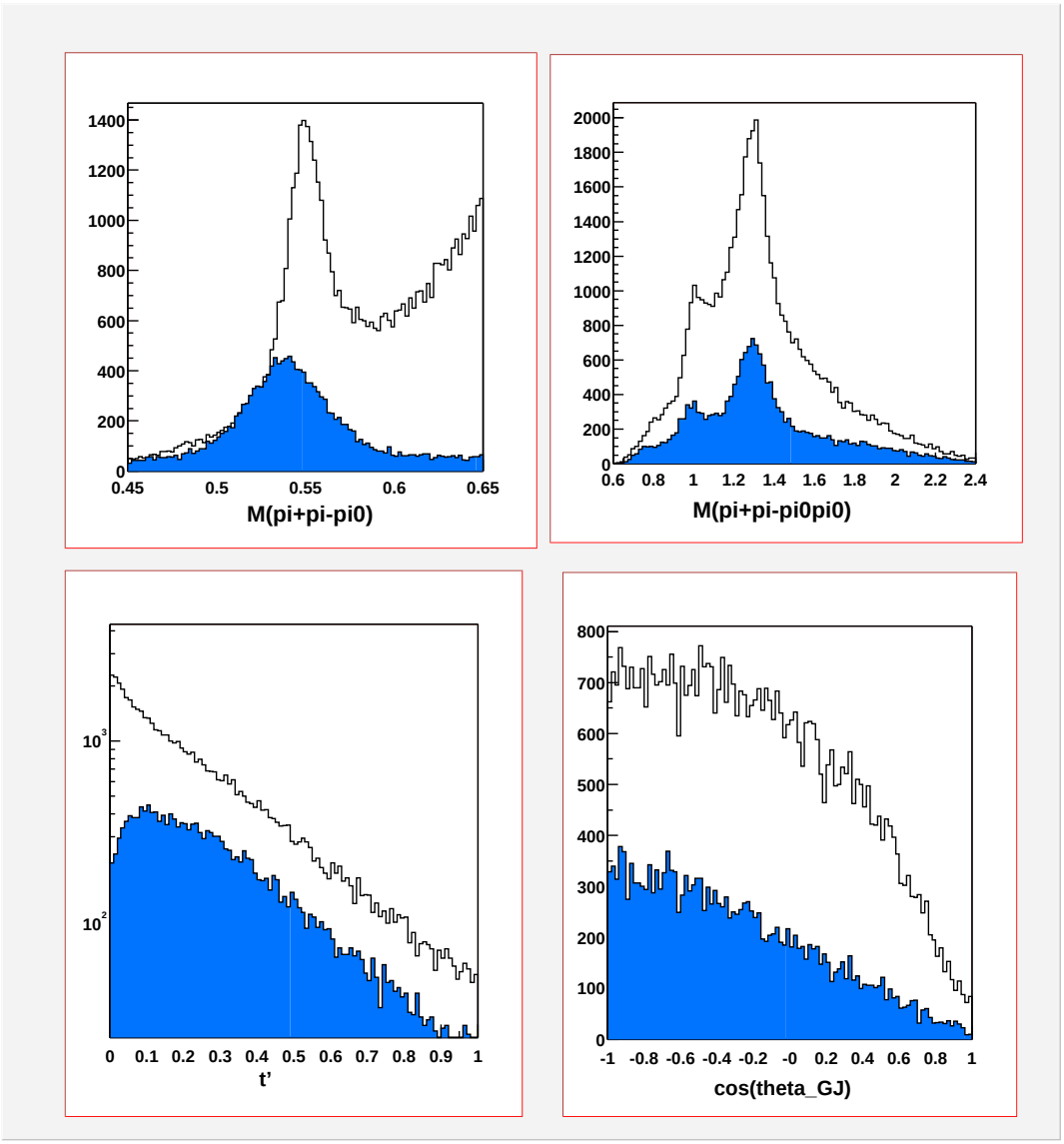

Figure 8: Three pion mass, four pion mass, t' - and $cos(\theta_{GJ})$ distributions. Hatched histogrames are after mass cut

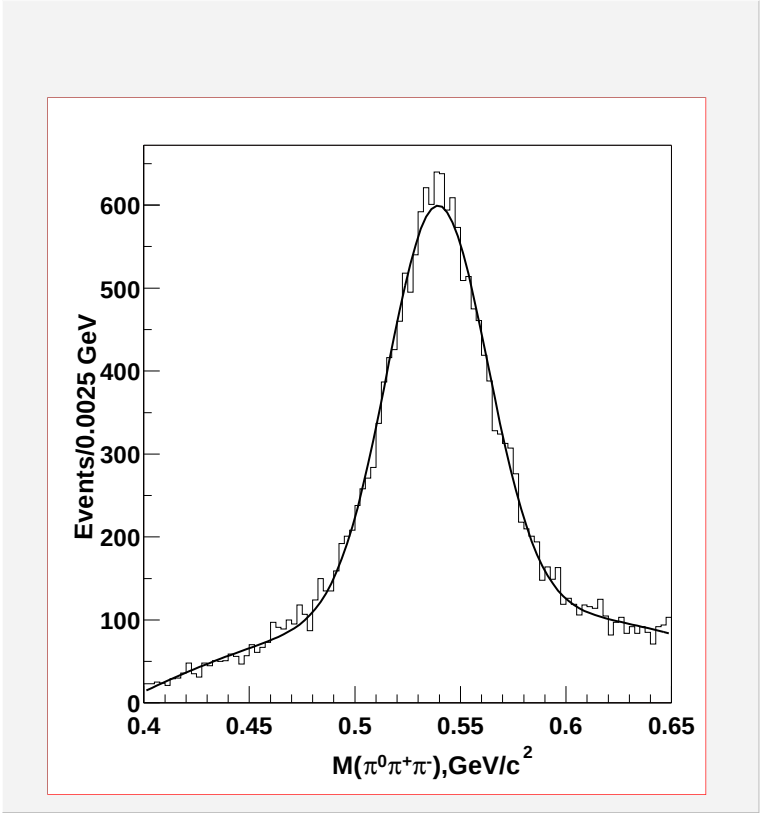

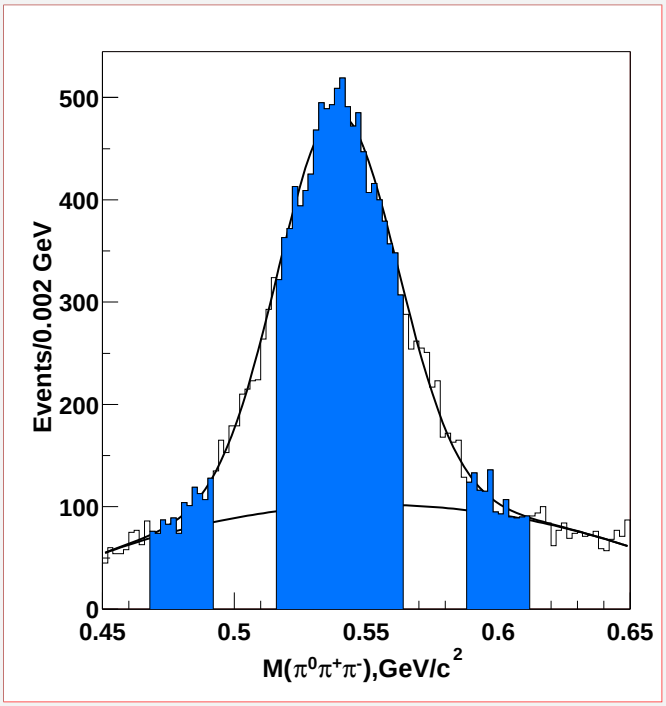

Figure 9: Fit of $\pi^0\pi^+\pi^-$ mass distribution in the η mass region

Figure 10: Selection of side bands in the $\pi^0\pi^+\pi^-$ distribution

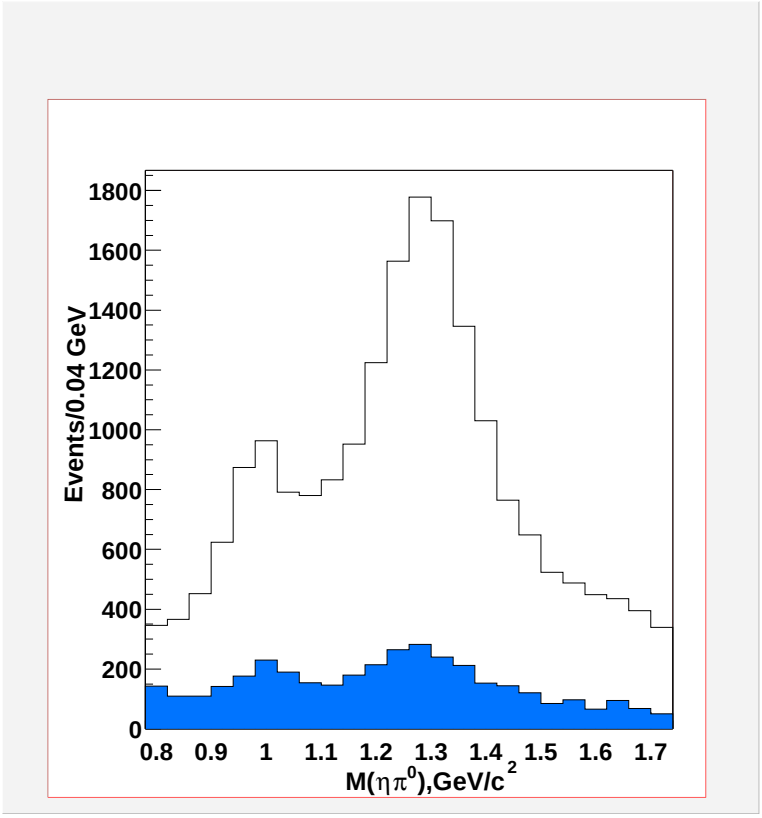

Figure 11: Data and background in the $\eta\pi^0$ mass distribution

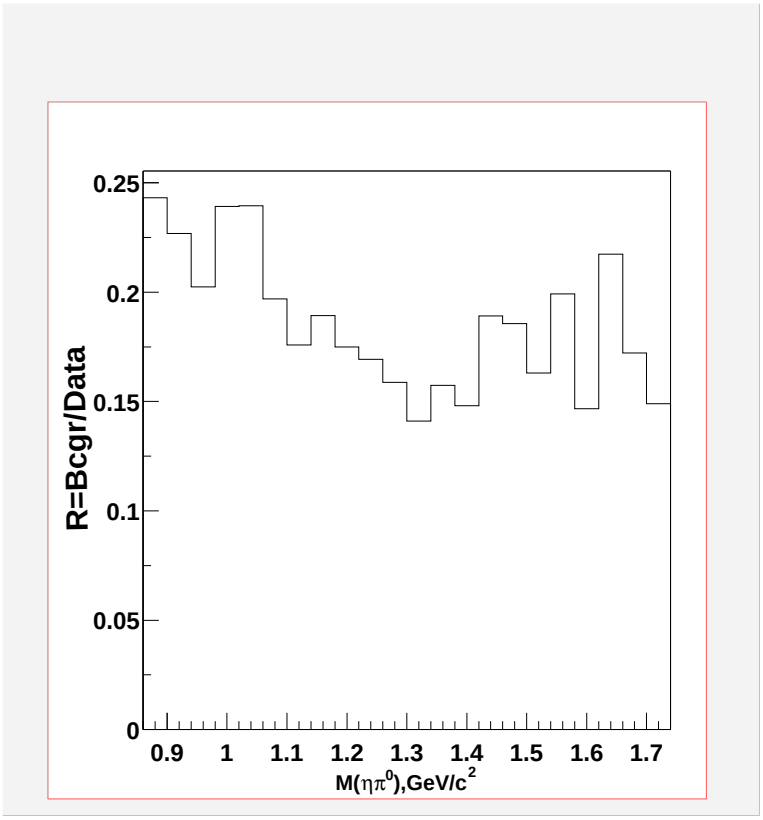

Figure 12: Ratio Bcgr/Data in the $\eta\pi^0$ mass distribution

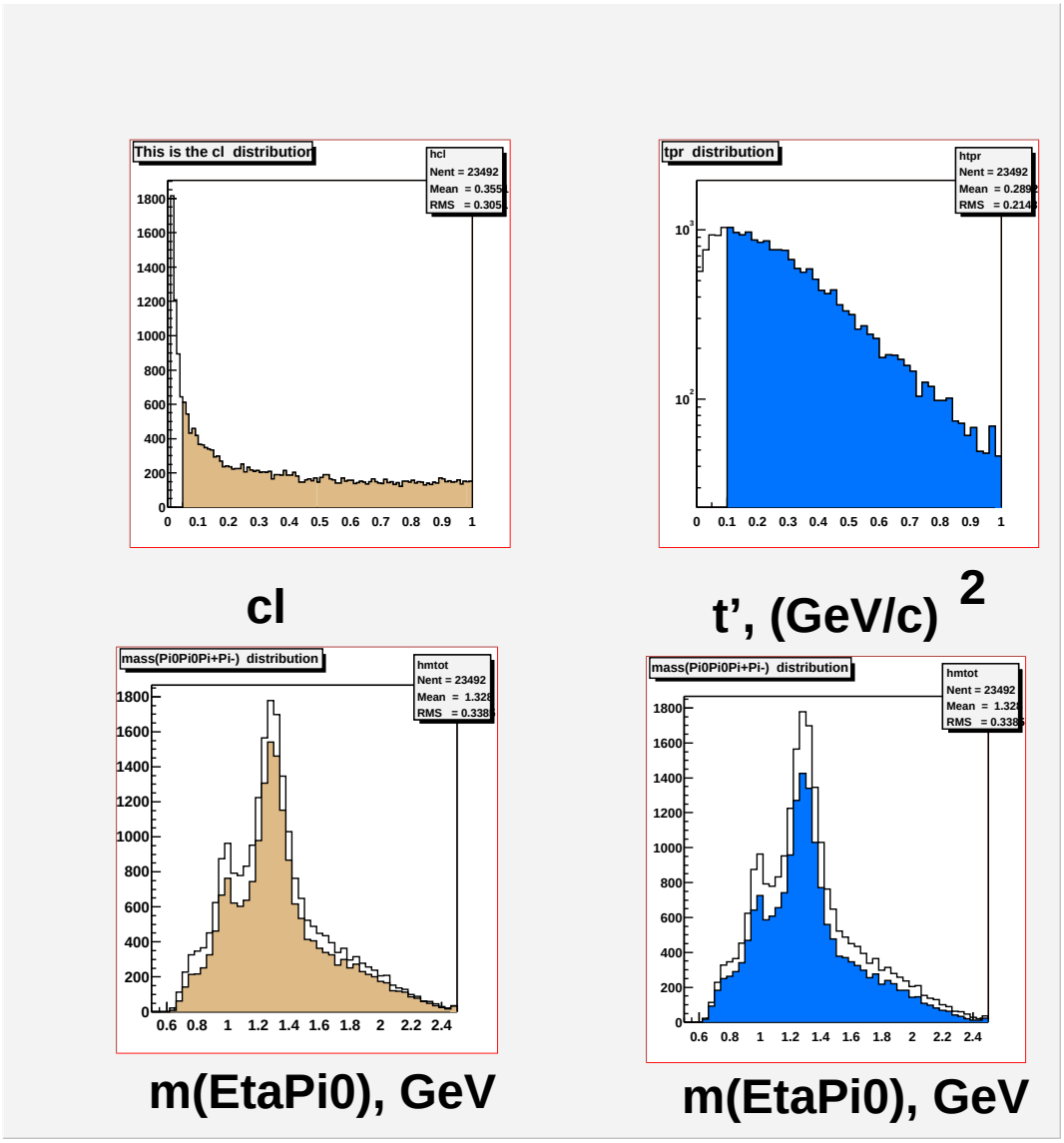

Figure 13: The distributions after SQUAW($\eta\pi^0$), a) cl - distribution, b) t' - distribution, c)mass($\eta\pi^0$) at $cl > 0.01$ and $cl > 0.05$, d) mass($\eta\pi^0$) at all t' and $t' > 0.1(GeV/c)^2$

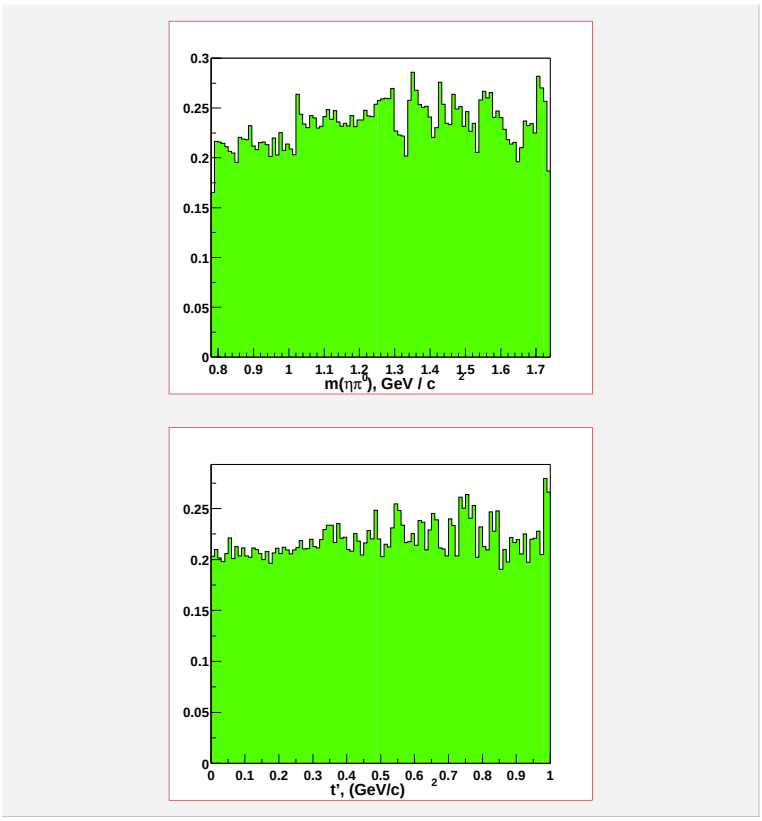

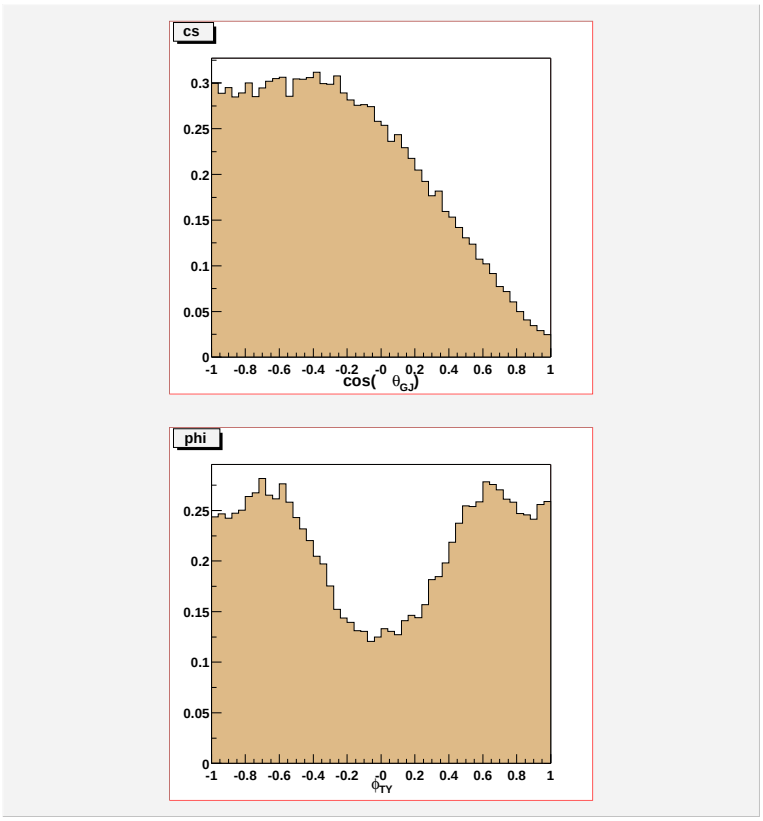

Figure 14: Acceptance of mass($\eta\pi^0$) and t' - distributions

Figure 15: Acceptance of $cos_{GJ}(\eta\pi^0)$ and $\phi_{TY}(\eta\pi^0)$- distributions

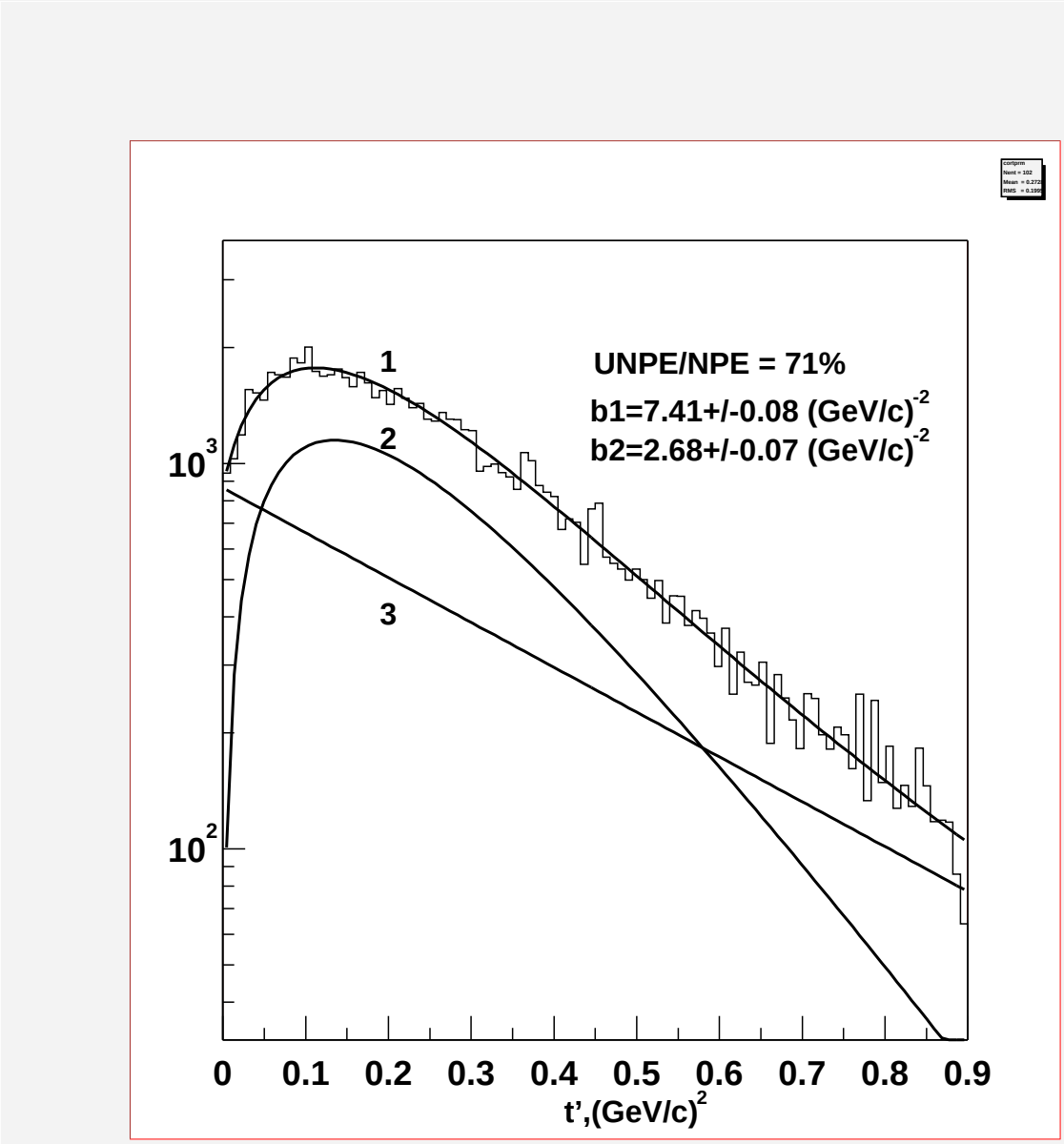

Figure 16: The acceptance corrected t' - distribution and the results of fit. 1) $N(t') = NPE + UNPE$, 2) $NPE = n_1|t'|e^{-b_1|t'|}$, 3) $UNPE = n_2 e^{-b_2|t'|}$

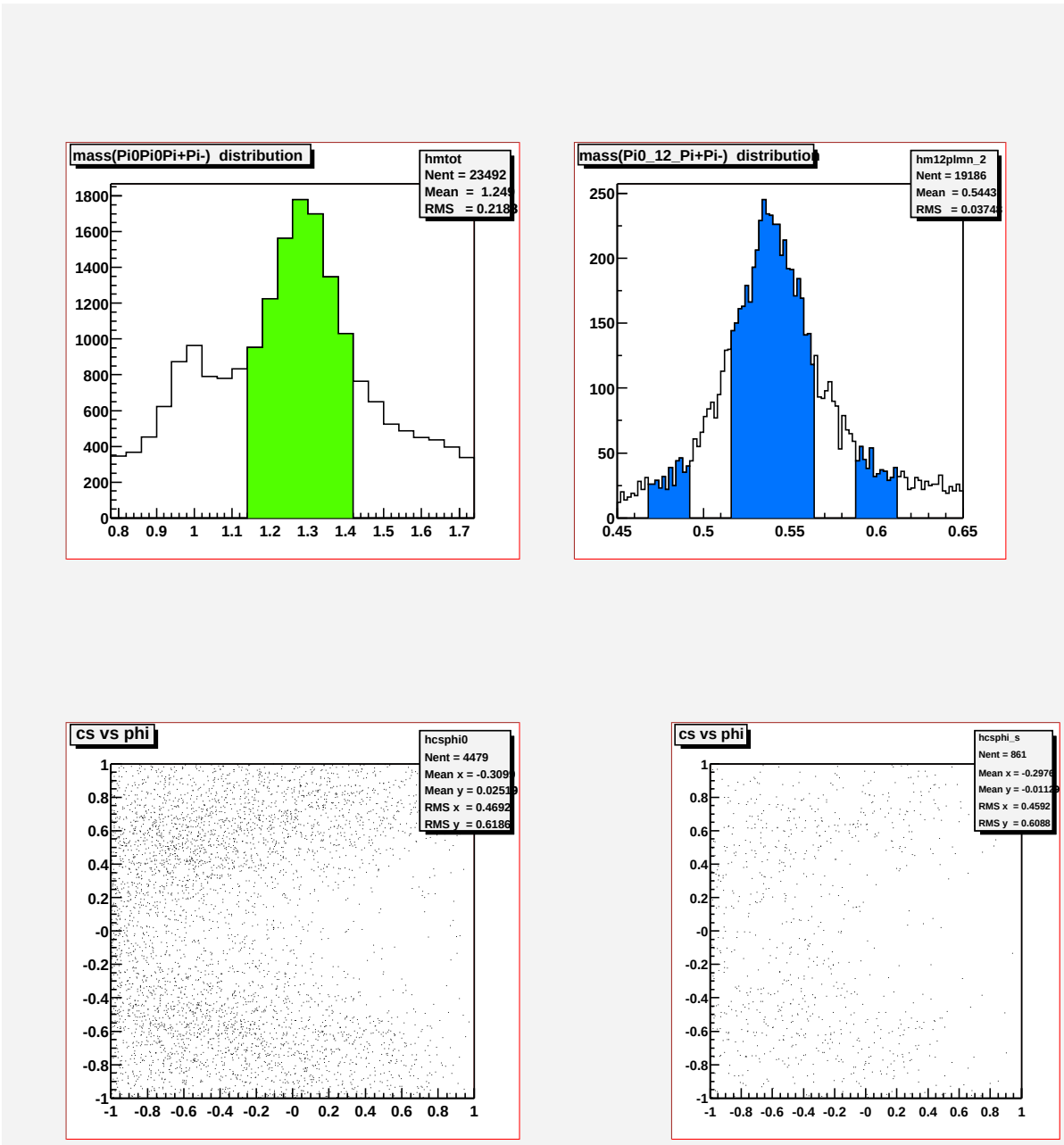

Figure 17: Two dimension ($\cos(\theta_{GJ})$, ϕ_{TY}) angular distribution for a_2 mass region: a) $M(\pi^+\pi^-\pi^0\pi^0)$ distribution and shadowed band for a_2 mass region, b)$M(\pi^+\pi^-\pi^0)$ distribution and shadowed band for η signal and side bands, c)($\cos(\theta_{GJ})$, ϕ_{TY}) for η mass region, d)($\cos(\theta_{GJ})$, ϕ_{TY}) for side bands

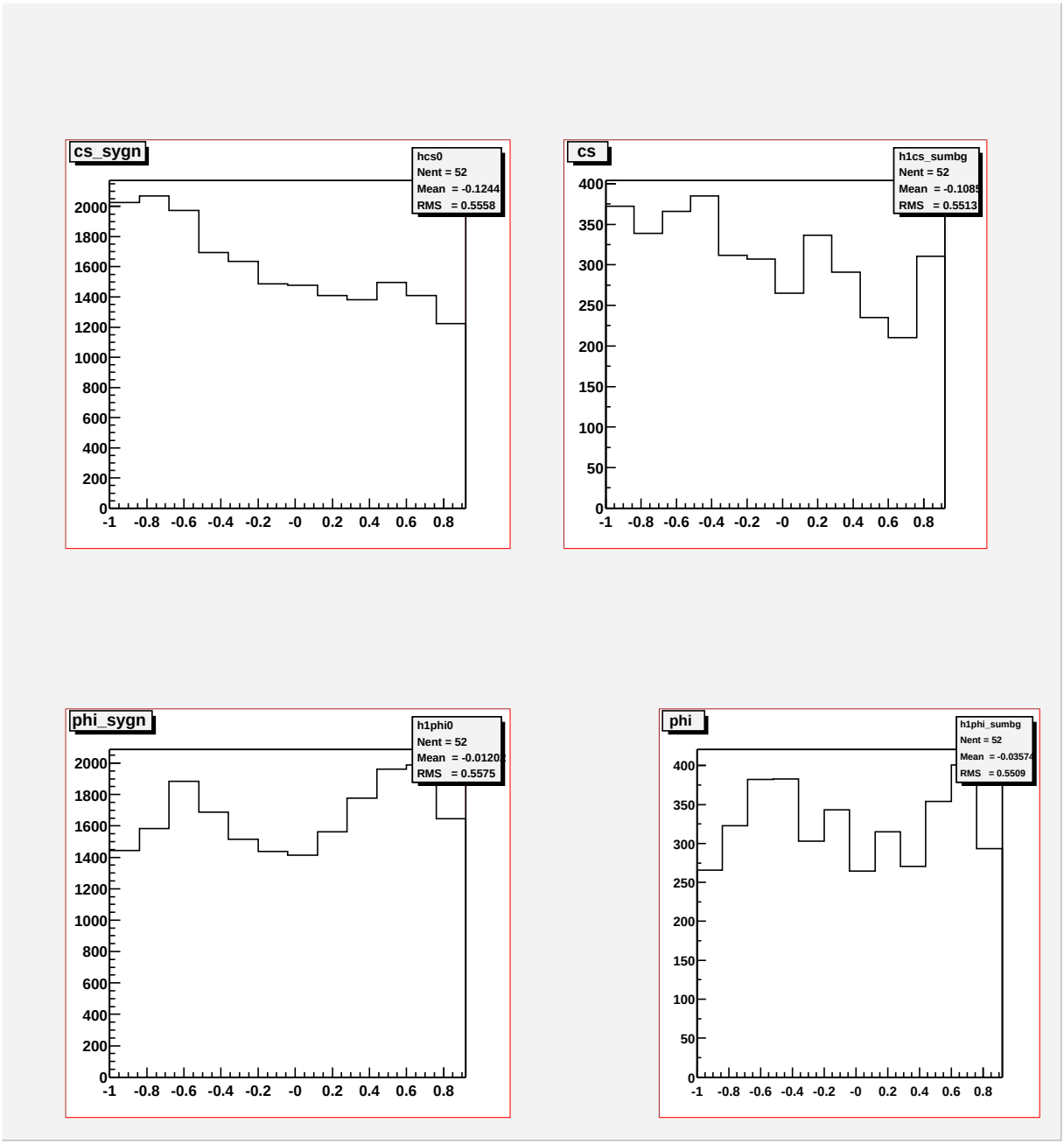

Figure 18: Acceptance corrected angular distribution for a_2 mass region 1.14-1.42 GeV. Upper raw is $\cos(\theta_{GJ})$ for a)η signal and b)side bands, low raw is ϕ_{TY} for c)η signal and c)side bands

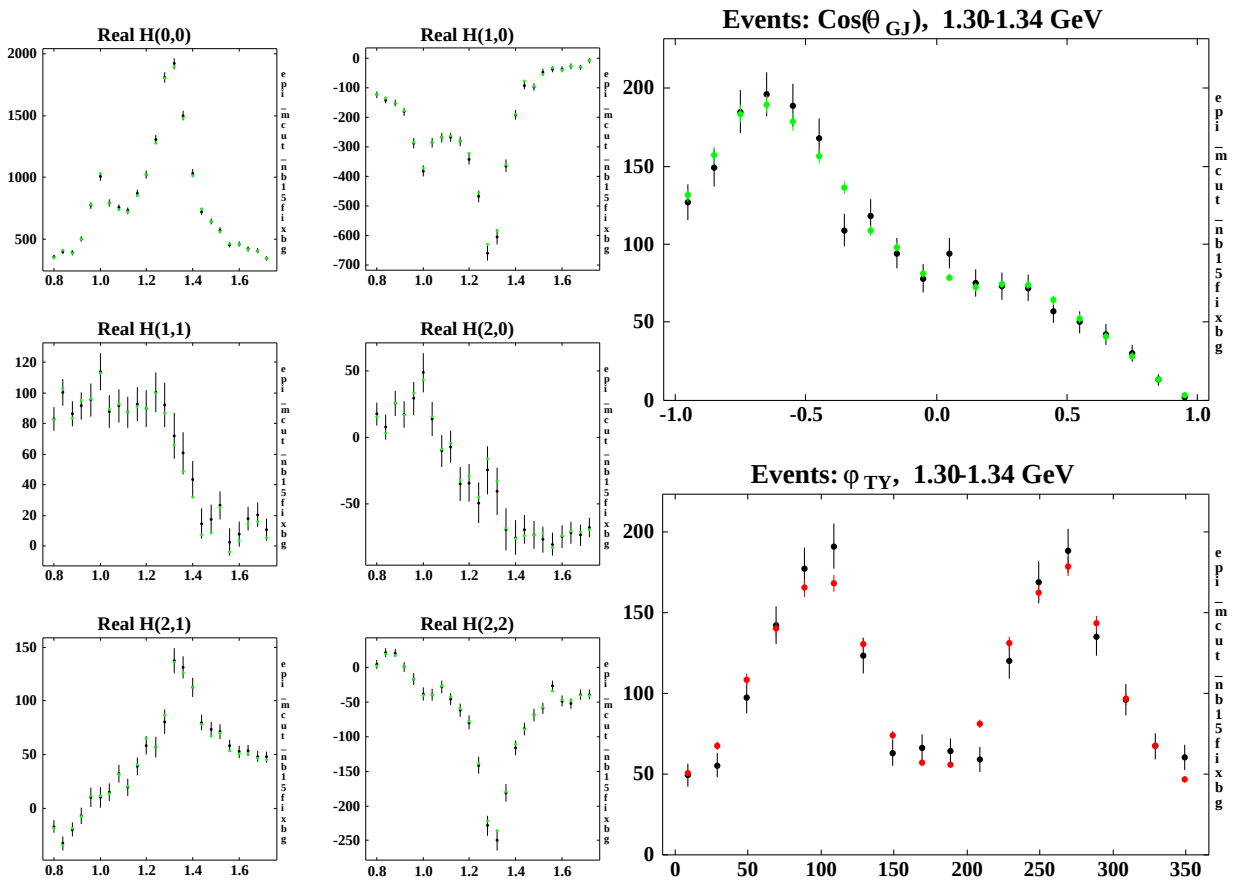

Figure 19: Experimental (points with errors) and the predicted moments H(LM).

Figure 20: Experimental and the predicted $cos(\theta_{GJ})$ and φ_{TY} for $1.30 < M(\eta\pi^0 < 1.34 GeV/c^2)$

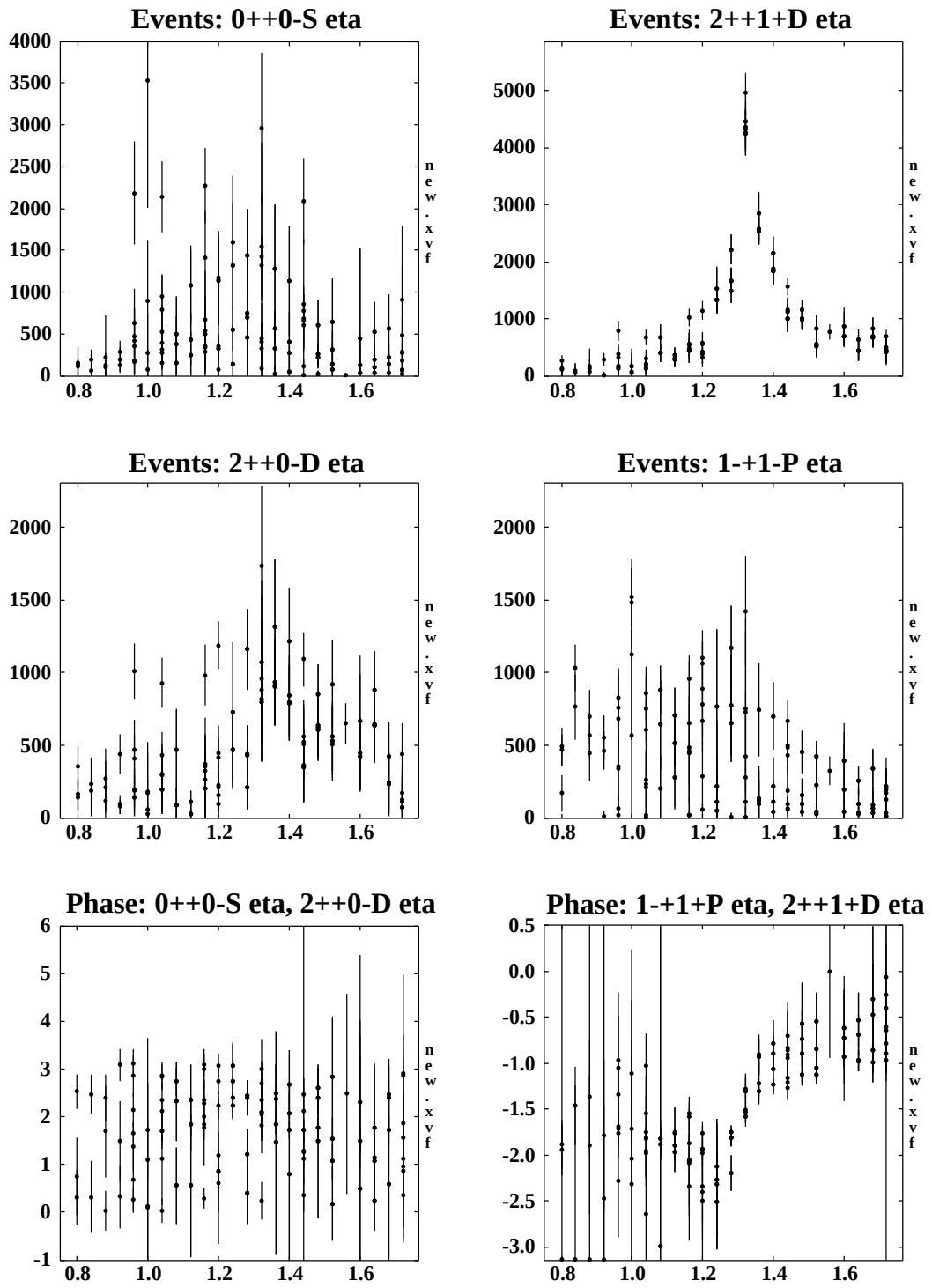

Figure 21: PWA of $\eta\pi^0$ system at fixed background. Mass ($\eta\pi^0$) distributions of waves: a) S_0, b)D_+, c)D_0, d)P_+, e)phase (S_0, D_0), f)phase (D_+, P_+)

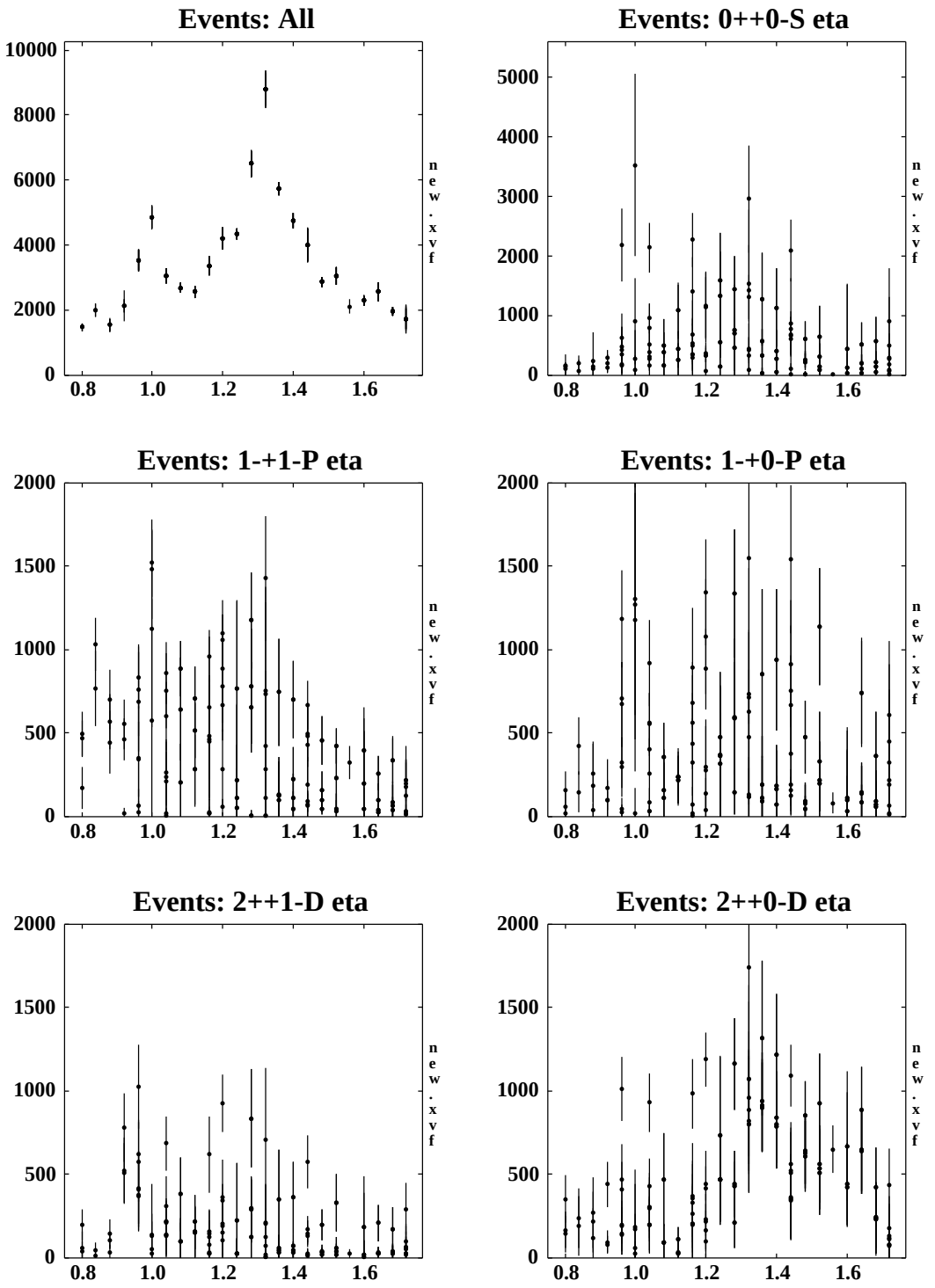

Figure 22: PWA of $\eta\pi^0$ system at fixed background. Mass ($\eta\pi^0$) distributions of waves: a) $Total$, b)S_0, c)P_-, d)P_0, e)D_-, f)D_0

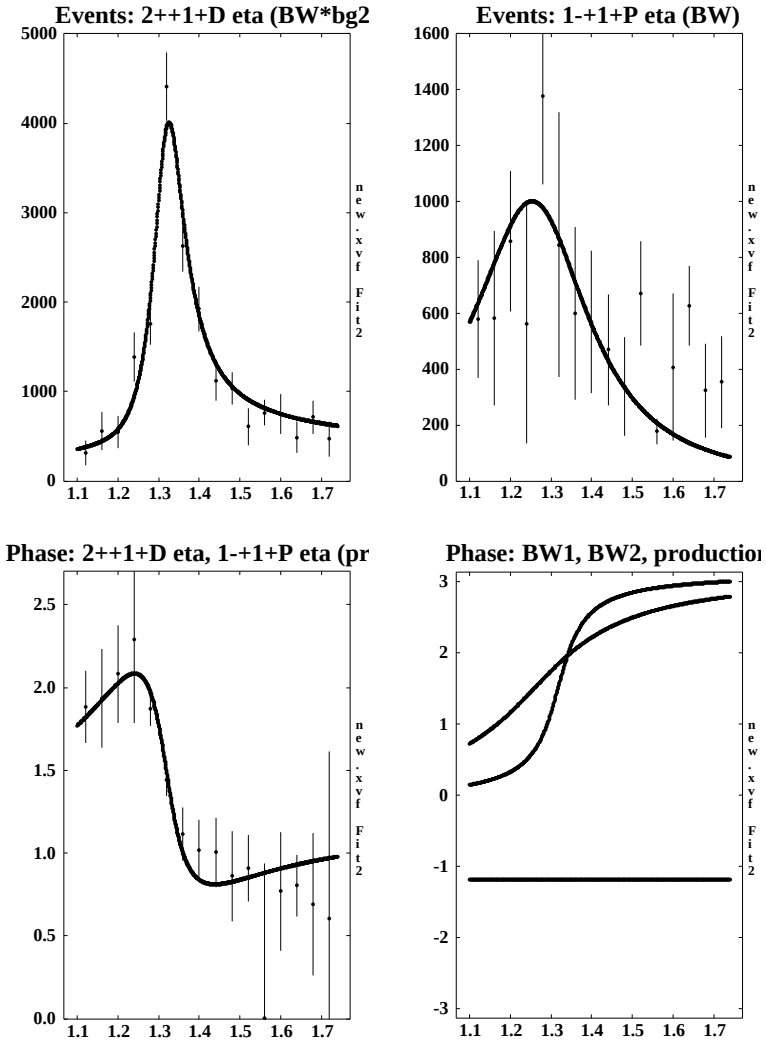

Figure 23: Mass dependent fit with the average solutions and error matrix of two resonant waves D_+ and P_+. a) D_+, b)P_+, c)relative phase (D_+, P_+), d) two BW and production phases.